# Machine Learned Potentials by Active Learning from Organic Crystal Structure Prediction Landscapes

Patrick W. V. Butler, Roohollah Hafizi, and Graeme M. Day*

*School of Chemistry, University of Southampton, Southampton, SO17 1BJ, United Kingdom*

E-mail: g.m.day@soton.ac.uk

## Abstract

A primary challenge in organic molecular crystal structure prediction (CSP) is accurately ranking the energies of potential structures. While high-level solid-state density functional theory (DFT) methods allow for mostly reliable discrimination of the low energy structures, their high computational cost is problematic because of the need to evaluate tens to hundreds of thousands of trial crystal structures to fully explore typical crystal energy landscapes. Consequently, lower-cost but less accurate empirical force fields are often used, sometimes as the first stage of a hierarchical scheme involving multiple stages of increasingly accurate energy calculations. Machine learned interatomic potentials (MLIPs), trained to reproduce the results of *ab initio* methods with computational cost close to that of force fields, can improve the efficiency of CSP by reducing or eliminating the need for costly DFT calculations. Here, we investigate active learning methods for training MLIPs with CSP datasets. The combination of active learning with the well-developed sampling methods from CSP yields potentials in a highly automated workflow that are relevant over a wide range of the crystal packing space. To demonstrate these potentials, we illustrate efficiently re-ranking large, diverse crystal structure landscapes to near-DFT accuracy from force field-based CSP, improving the reliability of the final energy ranking. Furthermore, we demonstrate how these potentials can be extended to more accurately model structures far from lattice energy minima through additional on-the-fly training within Monte Carlo simulations.

## Introduction

Molecular crystals are prevalent across a diverse range of materials applications, including opto-electronics, pharmaceuticals, and energetic materials.[1–3] The desirable properties of these materials are often strongly tied to the crystal structure—the arrangement of the molecules in the crystal lattice—and changes solely in the crystal structure can greatly affect a wide range of the physio-chemical properties of the crystals. This is seen clearly in polymorphs, which are crystals of the same compound but with different crystal structures.[4] The properties of polymorphs often differ substantially, such that the unexpected appearance of a polymorph can result in loss of control over material properties; the example of polymorphism in the drug Ritonavir illustrates the impact that this can have in pharmaceutical materials.[5] Polymorphs also offer an opportunity since they allow for materials to be potentially tuned to achieve enhanced properties.[6] Thus, predicting the crystal structure of molecular crystals has become a highly coveted goal and crystal structure prediction (CSP) is one of the primary challenges in materials science and computational chemistry.

CSP methods can conceptually be divided into two parts: first, the high-dimensional lattice energy space is comprehensively sampled to identify all relevant low energy, stable structures; and thereafter, the structures are ranked in terms of how likely they are to be observed. In general, the crystal structures are ranked based on thermodynamic stability. The resulting predicted landscapes typically contain hundreds to thousands of unique structures. As evidenced by the CSP blind tests, the best sampling methods have achieved maturity and reliably locate matches to experimental structures for rigid and moderately flexible molecules.[7–10] By contrast, determining the relative energy ranking of predicted organic crystal structures remains a notable challenge with often hundreds of distinct structures being within the typical energy range of polymorphism (˜7-8 kJ mol$^{-1}$)[11] above the global energy minimum. Differentiating these structures relies predominately on accurately evaluating the subtle balance of weak intermolecular interactions that holds organic crystals together. Additionally, thermal and entropic effects can be important for polymorphs close in energy. High level *ab initio* calculations provide a measure of consistency in identifying the balance of intermolecular forces.[12–18] However, these calculations have considerable computational cost and therefore are typically only applied to a subset of the predicted landscape, or are restricted to researchers with access to very large-scale computing resources.

The large cost of DFT calculations has resulted in pairwise atom-atom force fields with simple functional forms and multipole electrostatics remaining a fundamental part of CSP methods.[19] Indeed, because of the high number of crystal structures that must be evaluated, the initial energy surface that is sampled during the first stage of organic CSP is inevitably a force field energy surface. The effectiveness of CSP in finding good geometric matches to experimental structures thus reflects the generally good structures generated by these force fields. The relative energies calculated using the force fields applied during structure generation are equally important and, if not the final energies themselves, are the basis for selecting structures for further, higher level calculations. Therefore, it is desirable that these computationally cheaper methods are still as accurate as possible. However, fitting force fields that have high accuracy across diverse structures is challenging due to the simple functional form and compromises are often required.

A promising pathway to achieving the required high level accuracy of organic CSP at low cost is through the use of machine learned interatomic potentials (MLIPs) which, following training on *ab initio* reference data, can estimate energies and forces with the same level of accuracy but at a fraction of the cost.[20–24] Recent developments in both theory and computing hardware have led to MLIPs being widely adopted across materials modelling, including in CSP.[25–29] Their adoption for organic CSP, however, has been slower than other areas due to the unique challenges of these materials. Moreover, modern MLIPs in general rely on an axiom that the total energy can be decomposed into a sum of atomic energies, which are predicted based on local atomic environment descriptors. This particularly works well when the interaction is well-screened beyond the cutoff radius or when the bonding is homogeneous, as in inorganic materials. However, it cannot accurately capture interactions that occur on different scales, including the diversity of intermolecular interactions in organic crystals. Hence, while modern MLIPs excel at describing short range interactions, they often completely neglect the longer range interactions, including long-range dispersion and electrostatics, that extend beyond typical, computationally feasible cutoffs for the local atomic environment. Overcoming this limitation in order to capture all the relevant interactions in organic crystals requires either a more complex MLIP method,[30–32] or alternatively incorporation of a physical baseline that incorporates the missing long-range interactions.

A common approach to including a physical baseline is with $\Delta$-learning which, rather than learning total energies, focuses on learning the difference between a lower level method, such as a force field or Density Functional based Tight Binding (DFTB), and the higher level method, such as DFT. With the appropriate choice of the baseline, $\Delta$-learning combines the accurate description of long-range effects with the high-level accuracy of MLIPs for short range interactions, which can increase the accuracy of the final model with less data.[33] The validity of this approach has been demonstrated for organic crystals, with further extensions including multimer corrections and training separate models for the intramolecular and intermolecular components.[34–37]

Accurate MLIPs are also highly dependent on the training data collected. This is because the non-physical functional form of MLIPs means they are typically only accurate interpolating within regions of the energy surface covered by the training data. Consequently, generating comprehensive, representative, and diverse datasets is a non-trivial problem and a key concern for MLIP development. On one hand, large datasets allow MLIPs to cover a wide region of the energy landscape with high accuracy. On the other hand, large datasets are unfavorable because large numbers of expensive *ab initio* calculations are required and the computational cost of MLIP training increases. Furthermore, large randomly sampled datasets might introduce biases towards common configurations. A common approach to avoid these pitfalls is to apply an active learning approach, where structures are iteratively added to the training set from a large pool of candidates based on the model's predictions, with the model being retrained after each iteration to update the predictions.[25,38–48] There are various implementations of active learning. However, for MLIPs active learning often involves estimating the uncertainty of the predictions and adding structures with high uncertainty. Previous studies have found that active learning can significantly reduce the training set size required to achieve a certain level of accuracy of MLIP, reducing computational costs proportionally.[38]

Because active learning cannot increase the scope of the MLIP beyond that covered by the set of candidates, generating robust candidate datasets is still important. Molecular dynamics is one common method for generating these datasets. However, in the context of MLIPs for solid state systems, CSP landscapes can provide more diverse candidates, covering a wide scope of the potential energy surface (PES) and largely free of selection biases. As well as improving the efficiency of future CSP studies, MLIP training to CSP landscapes can leverage the excellent resource of already published CSP landscapes for those interested in developing MLIPs for crystal structure modelling.

In this contribution, we investigate how best to develop MLIPs, specifically neural network potentials (NNPs), from organic CSP landscapes. We begin by examining active learning on a CSP landscape of oxalic acid (Fig. 1a), investigating the effects of hyperparameters and strategies on the size and quality of the selected training set. From this we identify an efficient approach combining active learning with $\Delta$-learning. Thereafter, we demonstrate this approach through correcting to the DFT level CSP landscapes of resorcinol (Fig. 1b) and

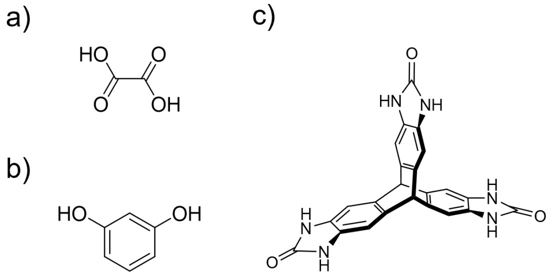

Figure 1: The compounds considered in this study: oxalic acid (a), resorcinol (b) and TTBI (c).

triptycene-tris(benzimidazolone) (TTBI, Fig. 1c), each containing thousands of structures. Finally, we detail how the potentials can be extended to describe structures far from the CSP minima by combining on-the-fly training with Monte-Carlo simulations. The scheme presented here provides access to MLIPs relevant over a wide scope of the crystal packing space and with the exacting accuracy required for organic CSP in a simple, efficient, and highly automated workflow.

# Methods

An overview of the workflow described here is shown in Figure 2. The fundamental idea consists of NNPs trained by active learning using query-by-committee (QBC) techniques to identify high uncertainty structures in CSP landscapes and Monte Carlo trajectories. The CSP landscapes can be explicitly calculated for this purpose or re-used from prior studies. In this work, only the oxalic acid landscape was calculated for the purpose of training NNPs. The more computationally demanding landscapes for resorcinol and TTBI were taken from earlier works.[49,50] All landscapes were originally generated by a quasi-random sampling of the crystal packing space using our Global Lattice Energy Explorer (GLEE) code.[51] The initial trial structures were generated from rigid molecules and lattice energy minimized using an empirically-parametrized *exp-6* potential consisting of the FIT[52–54] parameters for describing intermolecular exchange-repulsion and dispersion combined with atom-centered multipoles

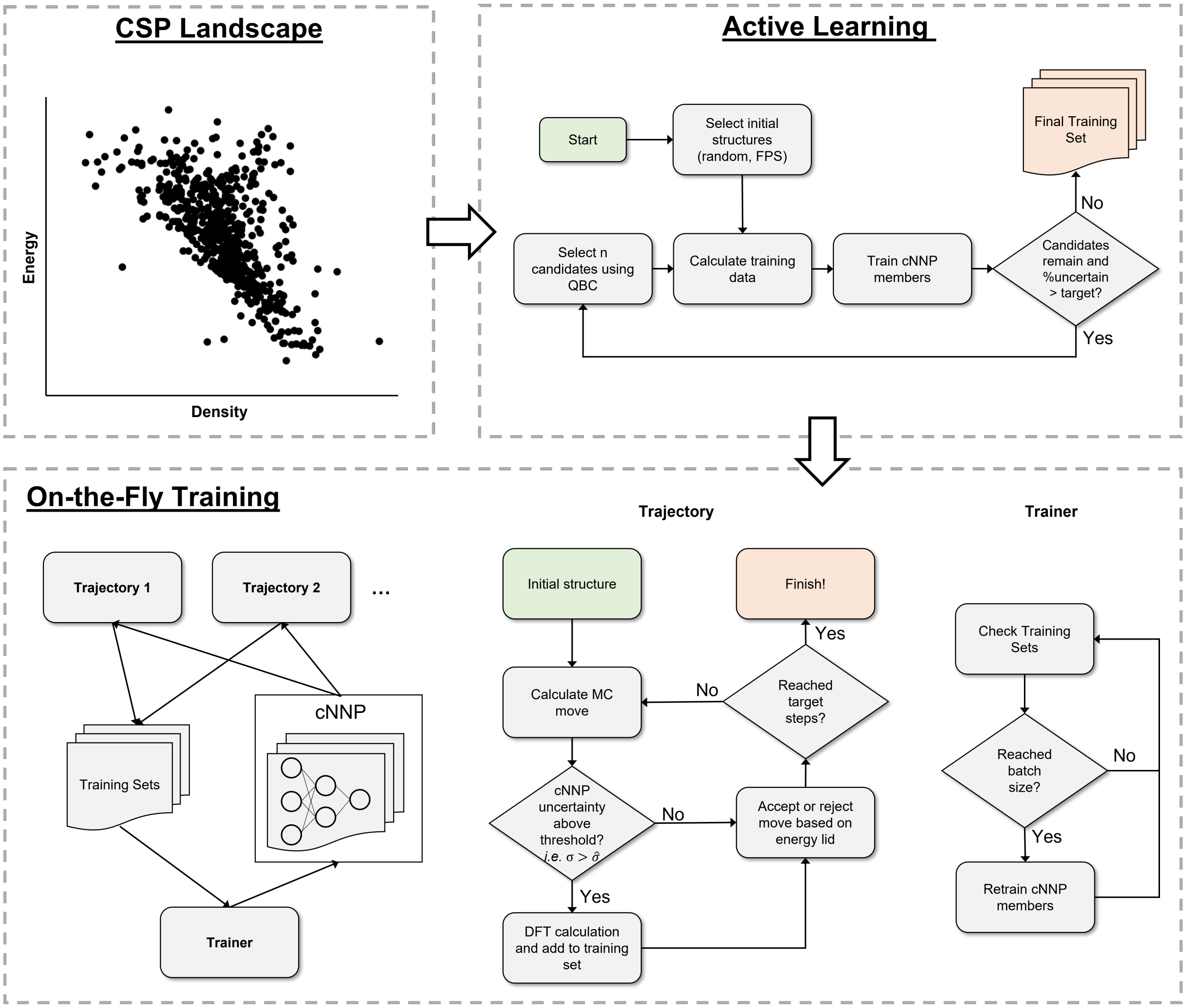

Figure 2: Overview of the workflow detailed. Starting from an initial CSP landscape the active learning flowchart describes how the final training set is produced. committee NNPs trained on this training set can then extended through on-the-fly training. The overview of the on-the-fly training and flowcharts for the trajectory and trainer subroutines are shown. Each subsection is automated and thus from CSP to on-the-fly training can be achieved with minimal intervention.

obtained from a distributed multipole analysis[55] (DMA) of the DFT-calculated molecular electron density (FIT+DMA). In the case of resorcinol, to account for the conformational flexibility, crystal structures were generated using a pool of rigid conformations and, following rigid-molecule lattice energy minimization, were fully relaxed at the dispersion-corrected DFTB level (DFTB-D3). Further details are provided in the supporting information.

Reference energies and forces were calculated with DFT using the PBE exchange correlation functional with the D3(BJ) dispersion correction (PBE-D3). This method is widely used as a first DFT approximation for molecular crystal lattice energies[10] The calculated reference data was used to train NNPs of the Behler-Parinello high-dimensional NNP form[56] as implemented in the n2p2 code.[57,58] The input to the NNPs are vectors of radial and angular atom-centered symmetry functions (ACSFs). ACSFs were selected from a larger set by a CUR decomposition following the procedure detailed by Imbalzano et al.,[59] which offers an improvement over a general set of symmetry functions (Table S1). For oxalic acid, a total of 64 radial and angular symmetry functions per element were selected, while for TTBI and resorcinol 128 total symmetry functions were selected. In all cases a maximum radial cutoff of 8.0 Å was used. Further details of the reference calculations and NNP models are provided in the supporting information.

## Query-By-Committee

As pure mathematical functions, neural networks do not natively estimate uncertainties in their predictions and thus various methods have been developed to provide these. A common approach with NNPs, and the one we use here, is to create committee neural network potentials (cNNP) and obtain uncertainties *via* QBC. This involves training an ensemble of n individual models, the committee, using the same dataset but with random variations in the initialisation of each member. Predictions are then made by averaging over the predictions of the individual members; for example energies are estimated as

$$E^{\,cNNP}(\mathbf{x}) = \frac{1}{n}\sum_{i=1}^{n} E_i(\mathbf{x}) \tag{1}$$

where $\mathbf{x}$ is the descriptor vector for a given structure and $E_i$ is the energy predicted by member $i$ of a committee of $n$ members. The uncertainty is derived from the standard deviation ($\sigma$) of the prediction between committee members. Since the true values will be precisely defined, high standard deviations imply high errors for one or more of the members, indicating the model is extrapolating beyond the training data and so reflecting the random variation between committee members. In addition to the uncertainty measure, by averaging over predictions, cNNPs have also been shown to have higher accuracy compared to a single NNP.[47] The caveat of cNNPs is an increased cost in training and predictions. This increase can be minimized through parallelization and by storing ACSF vectors.

## Active Learning from CSP Landscapes

Candidates indicated to have high uncertainty by QBC suggest regions of the configurational space that have not been learned sufficiently accurately given the current training set. Therefore, applying this to CSP landscapes we iteratively add predicted structures with high uncertainty to the training set. For the initial iteration, before the cNNP is first trained, we sample the candidates either randomly or by farthest point sampling (FPS), wherein additional structures are selected based on the maximum distance in the descriptor space from the previously selected structures (the first structure is selected randomly). While ideally the model would be retrained after each new structure is added to the training set, this has an impractically high computational cost in most cases and thus we define a batch size for how often the cNNP is retrained, i.e. the number of structures added at each iteration of active learning.

Another important parameter is the threshold for defining high uncertainty, $\hat{\sigma}$, which determines the structures that are added to the training set. Setting this parameter depends on the desired accuracy of the final model, but is typically complicated by not knowing the relationship between the variance in the cNNP predictions and the true error *a priori*. Here we define the uncertainty directly as the standard deviation of the cNNP prediction and set an uncertainty threshold in terms of the target energy units, kJ mol$^{-1}$ per molecule (abbreviated as kJ mol$^{-1}$ hereafter). While the uncertainties are uncalibrated, we find that a threshold of 1 - 2 kJ mol$^{-1}$, which is based on typical energy differences between polymorphs,[11] provides good accuracy for the systems studied. Candidates above the uncertainty threshold are added to the training set until either there are no more candidates or the percentage of candidates above the uncertainty threshold is below a specified target. Additionally, a maximum training set size can be set. The scheme is summarized in Figure 2 (top panel).

## On-The-Fly Training

The on-the-fly training scheme we propose here (the bottom panel of Figure 2) is based on threshold Monte Carlo (MC) simulations for sampling the configurational space. This method has been applied to molecular crystals using empirical force fields and DFTB to characterize the global structure of crystal energy landscapes[60] and to reduce overprediction of polymorphism.[49] These simulations involve regular MC sampling of the configurational space, but with the distinguishing feature of an energy lid, which is defined relative to the energy of the initial configuration from which the simulation was initiated. During the simulation MC moves are accepted if and only if the energy of the resulting structure is below the current energy lid. Consequently, the energy lid effectively constrains the simulation to explore only regions accessible below the lid, thereby providing a high level of control over the trajectory.

With on-the-fly training, each MC step is first evaluated by a cNNP. If the uncertainty of the predicted energy is above the specified threshold, the step is further evaluated by the reference method, in this case PBE-D3, and the configuration is added to the training set. The cNNP is constantly retrained as structures are added to the training set to ensure reliable uncertainties and avoid adding redundant structures. For the MC simulations described here we use a rigid molecule moveset consisting of molecular rotations and translations as well as unit cell lengths, angles, and volume changes. Conformational moves can be added to explore intramolecular perturbations to the crystal structure. Further details of the simulations are provided in the supporting information.

# Results

Table 1: Average MAE, RMSE, and dataset size with standard deviations from 5-fold cross-validation of combinations of active learning hyperparameters evaluated by training cNNPs with an oxalic acid CSP landscape. The cNNPs were trained either on total energy ($E$)/forces ($F$) or the difference between the CSP values and the reference values ($\Delta E/\Delta F$), i.e. $\Delta$-learning. All entries used an uncertainty cutoff of 1.0 kJ mol$^{-1}$ with candidates selected by highest uncertainty.

| Entry | Training Quantity | Committee Size | % Uncertain Target | Batch Size | Energy MAE (kJ mol$^{-1}$) | Energy RMSE (kJ mol$^{-1}$) | Final Training Set Size |
|---|---|---|---|---|---|---|---|
| 1 | $E$ | 6 | 10.0 | 30 | 1.11 (0.05) | 1.74 (0.18) | 852 (24) |
| 2 | $E$, $F$ | 6 | 10.0 | 30 | 1.08 (0.10) | 1.50 (0.13) | 546 (40) |
| 3 | $\Delta E$ | 6 | 10.0 | 30 | 1.09 (0.11) | 1.47 (0.18) | 205 (53) |
| 4 | $\Delta E$, $\Delta F$ | 6 | 10.0 | 30 | 0.92 (0.06) | 1.20 (0.07) | 216 (22) |
| 5 | $\Delta E$ | 6 | 2.5 | 30 | 0.89 (0.11) | 1.21 (0.20) | 354 (72) |
| 6 | $\Delta E$ | 6 | 5.0 | 30 | 0.97 (0.06) | 1.29 (0.10) | 252 (45) |
| 7 | $\Delta E$ | 2 | 5.0 | 30 | 1.19 (0.18) | 1.61 (0.26) | 168 (65) |
| 8 | $\Delta E$ | 18 | 5.0 | 30 | 0.90 (0.06) | 1.20 (0.12) | 288 (41) |
| 9 | $\Delta E$ | 6 | 5.0 | 15 | 1.01 (0.05) | 1.37 (0.17) | 216 (15) |
| 10 | $\Delta E$ | 6 | 5.0 | 60 | 0.90 (0.08) | 1.38 (0.43) | 320 (45) |

## Optimising Active Learning for CSP Landscapes

A primary consideration when developing machine learned models is determining an appropriate set of hyperparameters. For an MLIP there are hyperparameters for the model, such as the network architecture of NNPs, as well as hyperparameters for the descriptor, for example the radial cutoff. Active learning has its own hyperparameters, including the batch size and uncertainty threshold, and also a query strategy. In order to apply active learning efficiently with CSP datasets we first investigated optimising the hyperparameters and selection strategy. The aim was to identify the approach that yields the smallest training set that accurately captures the whole landscape, as measured by small test errors, and does so consistently with minimal variation.

The dataset we chose for these studies was a predicted landscape for oxalic acid containing 1965 crystal structures. We chose this landscape because oxalic acid is a known challenging system for empirical force fields[61] and thus learning either the total energy or $\Delta$-learning the correction from force field to DFT will be meaningful tests. Furthermore, the small size of the oxalic acid structures meant calculating the entire dataset at the target level, PBE-D3, was possible, and thus results were able to be verified through 5-fold cross-validation.

### Hyperparameters

The hyperparameters we chose to investigate for optimisation were: the target quantity, the committee size, the batch size, and the target percentage of structures above the uncertainty threshold. The results of varying these parameters individually with 5-fold cross validation are shown in Table 1. In all cases the uncertainty threshold was set at 1.0 kJ mol$^{-1}$ and structures were added to the training set by highest uncertainty.

The most influential hyperparameter on the final training set is the training quantity (compare entries 1-4, Table 1). $\Delta$-learning dramatically reduces the size of the training set, by up to 76%, while achieving similar if not better accuracy than learning the total energy (or energy and forces). Importantly, the improvement was similar if restricted to training only on the energy differences without forces, which is expected to be a common application since atomic forces are often not stored with CSP landscapes. However, if atomic forces are available, including these in the training is likely worthwhile and would yield an improved description of the energy surface around the lattice energy minima, which may be important for further calculations beyond the lattice energy correction, for example calculations of vibrational modes. Compared to the training quantity, the other hyperparameters are less significant, yet tuning these parameters does offer notable improvements, particularly in the efficiency. For example, we found that a large NNP committee of 18 members does not offer significant improvement over a smaller committee of 6 members despite incurring significantly greater costs. The improved average errors with the 18 member committee are within that expected due solely to a larger committee (Figure S2), suggesting the dataset chosen by active learning is not higher quality. Moreover, while smaller committees could provide adequate results they were found to generally underestimate the standard deviation

(Table S3) and thus the uncertainty. Similar trends of diminishing returns are observed in the other hyperparameters studied. Overall, we identify the parameters of entry 6 as the best balance between accuracy and cost and we use these settings in the following sections.

Table 2: Results of 5-fold cross validation for the active learning strategies evaluated by training cNNPs with an oxalic acid CSP landscape. All cases used the active learning hyperparameters in entry 6 of table 1 with the uncertainty threshold of 1 kJ mol$^{-1}$.

| Strategy | Energy MAE (kJ mol$^{-1}$) | Energy RMSE (kJ mol$^{-1}$) | Final Dataset Size |
|---|---|---|---|
| Random | 0.86 (0.04) | 1.20 (0.13) | 320 (36) |
| Highest Uncertainty | 0.97 (0.06) | 1.29 (0.10) | 252 (45) |
| Highest Uncertainty FPS | 0.96 (0.10) | 1.33 (0.16) | 288 (67) |

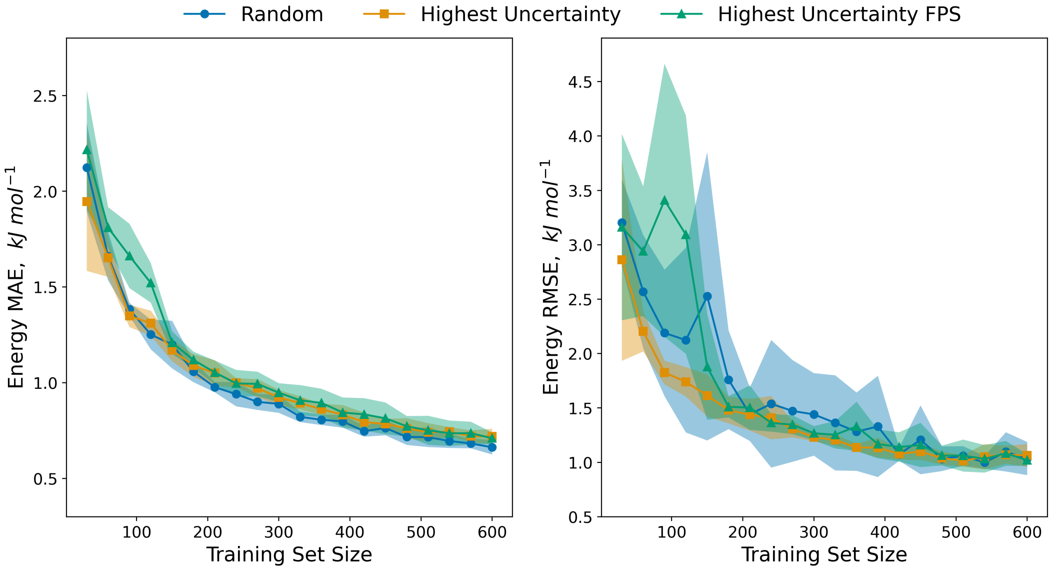

Figure 3: Learning curves in energy MAE (left) and energy RMSE (right) from 5-fold cross validation for the three strategies. Average values across the 5 folds are indicated by solid lines while the shaded area represents one standard deviation. Active learning hyperparameters are the same as entry 6 of table 1, except the uncertainty cutoff was decreased to 0.5 kJ mol$^{-1}$ to extend the active learning to training set size of 600 across folds.

## Query Strategies

We also investigated different strategies for adding candidates to the training set, beginning with comparing active learning random sampling and highest uncertainty sampling. The former involves evaluating each candidate once, in random order, and adding those above the uncertainty threshold to the training set, retraining when reaching the batch size. By contrast, highest uncertainty sampling, which is the most common strategy for MLIPs, evaluates all remaining candidates each iteration and adds the candidates with the highest uncertainty to the training set. Additionally, we implemented a strategy combining highest uncertainty and farthest point sampling. This strategy, which sampled candidates above the uncertainty threshold by FPS starting from the candidate with the highest uncertainty, was intended to reduce redundancy in the training set that may arise when sampling by highest uncertainty with a batch size greater than one.

Comparing these strategies by 5-fold cross validation, we found their performance to be similar (Table 2). On average the highest uncertainty sampling converged fastest, but with the smaller dataset also had on average higher errors than random sampling. The training curves (Fig. 3) make the differences between strategies clearer. Here we found the highest uncertainty sampling had faster convergence with significantly smaller variance as measured by both MAE and RMSE. By contrast, random sampling RMSE converged slower and with higher variance even at large dataset sizes. Interestingly, the highest uncertainty FPS strategy did not show improvement over regular highest uncertainty sampling. This may indicate that the weighting of FPS and highest uncertainty sampling needs adjusting. Nevertheless, the results suggests that there is no significant benefit of the strategy over regular highest uncertainty sampling, which from the oxalic acid results is the best of the three strategies for training cNNPs from CSP datasets.

## Correcting Low-Level CSP landscapes to *ab initio* Level

Due to the exacting accuracy required, a primary task in organic CSP is correcting lower level landscapes to higher levels of theory. This may also include re-optimization of the geometries of predicted structures. However, single point corrections are also common, where the geometries not updated when energies are re-evaluated at the higher level. The latter correction is especially relevant for MLIPs trained by $\Delta$-learning from CSP landscapes. To investigate this application, we applied our active learning workflow detailed in the previous section to the CSP landscapes of two challenging systems – TTBI and resorcinol – and then used the resulting training set to train cNNPs to generate corrected landscapes. The final cNNPs consisted of 18 members since these provide slightly better prediction averages over the 6 member committees used in the active learning (Figure S2) and has negligible cost post-active learning.

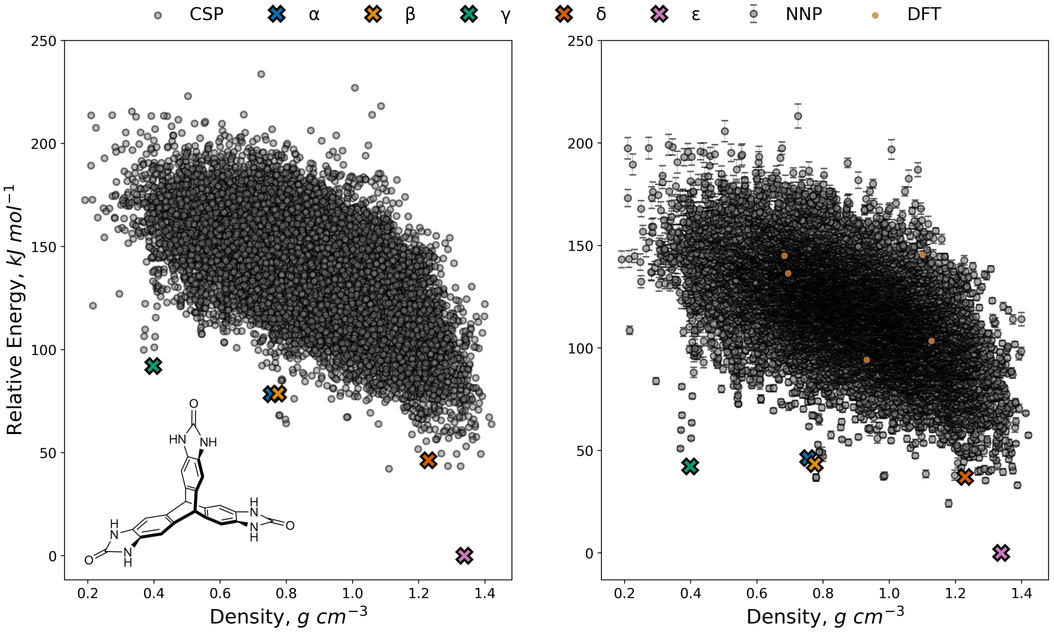

Figure 4: FIT+DMA landscape (left) and cNNP re-ranked landscape (right) for TTBI. Error bars on cNNP energies correspond to the standard deviation in the committee predictions. Structures with energies beyond 250 kJ mol$^{-1}$ above the global minimum have been omitted for clarity. Structures marked with an X correspond to experimentally observed polymorphs. Yellow markers indicate structures with high uncertainty ($>$ 6 kJ mol$^{-1}$) which were evaluated directly with the target method.

### triptycene-tris(benzimidazolone) (TTBI)

The first application we describe is for TTBI, a triptycene derivative with five known polymorphs and a propensity for forming highly porous, hydrogen-bonded organic frameworks.[50,62,63] The initial landscape used to train the cNNP was reported by Zhu et. al.[50] and was produced using the FIT+DMA potential, which does an adequate job at identifying the experimental structures and separating them from the bulk of the predicted structures. However, the relative energy differences between the polymorphs are questionable with the gap between the global energy minimum structure (corresponding to the densely-packed $\epsilon$ polymorph) and the least dense porous $\gamma$ polymorph at nearly 100 kJ mol$^{-1}$. Although solvent incorporated in the voids was shown to stabilize the porous polymorphs during growth,[63] the FIT+DMA polymorph energy differences seem unreasonably large energy. The relative energies are also sensitive to the calculation method: DFTB-D3 optimization reduces the energy gap between the polymorphs,[50] as do predictions using the W99+DMA force field.[63] Understanding the achievable energetic range for metastable crystal structures with attractive properties is important for developing CSP for materials discovery. However, calculating higher level energies for such CSP landscapes has thus far been too computationally expensive due to both the large size of the structures and the scale of the landscape: the TTBI CSP landscape used here contains 14997 distinct structures. Furthermore, the landscape exhibits a diverse range of structures covering a very wide density range and from primarily dispersion-bound structures to hydrogen bonded structures: this diversity in intermolecular interactions is a further challenge to training a MLIP to predict accurate energies.

Considering the results of our hyperparameter and strategy tests, we performed the active learning with a committee of 6 NNPs, training on $\Delta E$, and adding structures by highest uncertainty. Due to the larger size of the structures (46 atoms/molecule), the uncertainty threshold was set at 2 kJ mol$^{-1}$ per molecule and batch size set to five structures. Furthermore, to focus the potential towards the lower energy structures we applied a cutoff at 110 kJ mol$^{-1}$ above the global energy minimum, which gave 2220 candidate structures for training and included all matches to the experimental polymorphs.

With these settings, the active learning converged in 185 structures, corresponding to less than 10% of the candidates and only 1.2% of the total landscape. The corrected landscape calculated with the final potential is presented in Figure 4, the uncertainties represented by error bars on each structure. Despite the energy cutoff and small training set, the potential achieves good accuracy across the entire landscape: only 9 out of the 14997 structures had uncertainties above 6 kJ mol$^{-1}$. The energies of these structures were computed directly with PBE-D3. Pleasingly, the correction yields a considerable reduction in the energy range of the experimentally observed polymorphs, the gap between the global minimum and the low density ($\alpha$, $\beta$ and $\gamma$) polymorphs reducing to less than 50 kJ mol$^{-1}$, which is in line with the solvation stabilization estimated for these structures.[64] Comparing the corrected energies to calculated PBE-D3 energies for 92 of the lowest energy structures on the initial landscape (16 of which were selected by active learning), we find an MAE of 3.1 kJ mol$^{-1}$ and an RMSE of 4.1 kJ mol$^{-1}$ (Figure S3). In terms of energy rankings, following the correction all five known polymorphs are ranked in the 30 lowest energy structures with the biggest change in rank being observed for the very low density $\gamma$ polymorph, which dropped from 647$^{th}$ to 21$^{st}$ on the landscape. This remarkably good ranking of the polymorphs with such a minimal training set is highly encouraging for the application of the active learning workflow to other diverse, large scale landscapes, and highlights the advantage of the correction even for landscapes where the low level method is initially thought to perform reasonably well.

### Resorcinol

We next investigated applying the active learning workflow to resorcinol, a small organic molecule that has been well-studied as an example of conformational polymorphism. The initial CSP landscape, which was calculated from a pool of conformations and relaxed at the DFTB-D3 level, contains matches to the observed $\alpha$ and $\beta$ polymorphs. The molecules in these polymorphs differ conformationally by rotation of one hydroxyl group 180°, transforming between *syn*-*syn* and *syn*-*anti* conformations. This conformational flexibility means that, whereas the models trained for oxalic acid and TTBI were effectively intermolecular potentials, correcting the resorcinol landscape requires training a model that describes both intramolecular and intermolecular energy corrections. To add to this, the DFTB-D3 description of the relative energies of the resorcinol structures contains clear deficiencies and

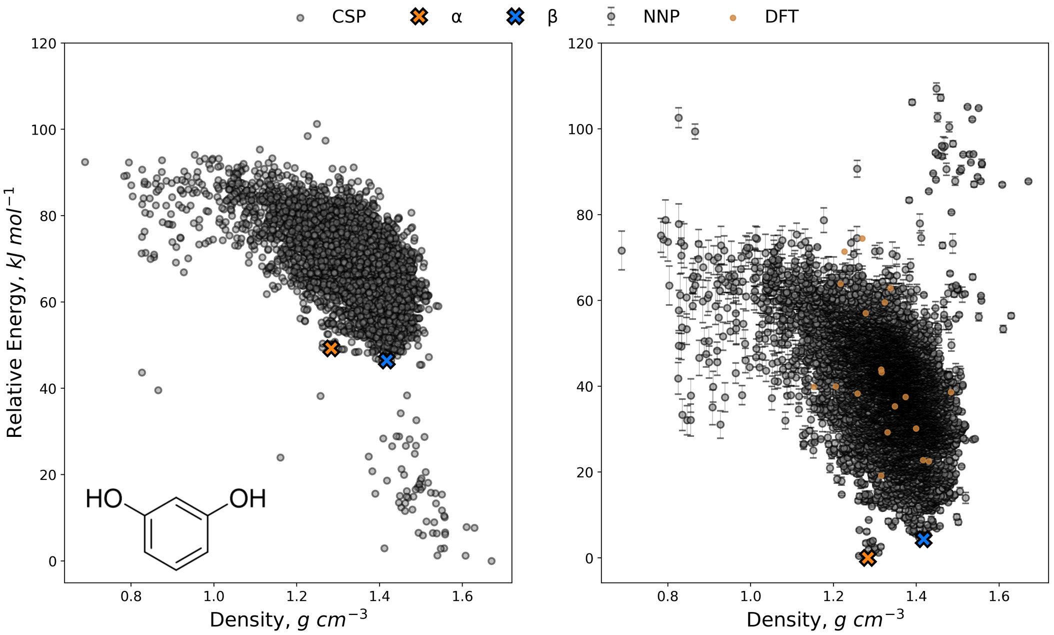

Figure 5: DFTB-D3 landscape (left) and cNNP re-ranked landscape (right) for resorcinol. Error bars on cNNP energies correspond to the standard deviation in the committee predictions. Structures marked with an X correspond to experimentally observed polymorphs. Yellow circles indicate structures with high uncertainty ($>$ 6 kJ mol$^{-1}$) which were evaluated directly with the target DFT method.

correlates poorly with the target PBE-D3 relative energies (Figure S2), which increases the difficulty of learning the correction. It is also notable that the DFTB-D3 landscape incorrectly ranks the $\beta$ polymorph lower in energy than the $\alpha$ polymorph, opposite to the expected order.

While the smaller size of the resorcinol structures means directly calculating the higher level landscape is possible, the large size of the landscape, containing 8808 structures, means this would still be quite costly. Therefore, this landscape is suitable for applying the active learning workflow, and moreover, considering the conformational flexibility and poor relative energies we envisaged this landscape to be a significant test of the active learning workflow and the resulting NNP.

The active learning was performed with the same settings as for TTBI, except in this case the uncertainty threshold was set to 1.0 kJ mol$^{-1}$ and the batch size to 15 structures. A cutoff at 65 kJ mol$^{-1}$ above the global minimum was applied, resulting in a candidate pool of 2487 structures, which contained matches to both the $\alpha$ and $\beta$ polymorphs.

With these settings, active learning completed after adding 780 structures, i.e. 31% of the candidates and 9% of the total landscape. This is significantly higher than seen for oxalic acid or TTBI, illustrating the impact of a poor correlation between the baseline (DFTB-D3) and target (PBE-D3) methods, increasing the complexity of the function that the model is attempting to fit. The corrected landscape evaluated with the final potential is presented in figure 5. Out of the 8808 structures, 19 had uncertainties above 6 kJ mol$^{-1}$ and were evaluated directly with the target method. Examining these structures, most were only slightly above the threshold and the predicted energies were close to the computed energies, suggesting that the cutoff at 6 kJ mol$^{-1}$ may have been tighter than needed.

Comparing the corrected with the initial DFTB-D3 landscapes, we can see many of the deficiencies from the baseline (DFTB-D3) landscape have been eliminated. The structures corresponding to the experimentally observed polymorphs are now among the lowest energy structures on the landscape and in the correct expected order of stability, the $\alpha$ polymorph being the global minimum and the $\beta$ polymorph ranked slightly higher. The CSP structures that were predicted with low energies and high densities by DFTB-D3 have been corrected to higher energies, and now are the highest energy structures on the landscape, emphasizing the very poor description of these structures on the initial landscape. Despite the large correction required, for the vast majority of the landscape the potential estimates the corrections with low uncertainty, the mean uncertainty being 1.51 kJ mol$^{-1}$. Moreover, comparing the corrected energies to the calculated PBE-D3 energies for the 300 lowest energy structures on the initial landscape (106 of which were selected by active learning), we find an MAE of 0.4 kJ mol$^{-1}$ and an RMSE of 0.6 kJ mol$^{-1}$ (Figure S2). The only notable exceptions are the low density CSP structures, which have larger uncertainties. This is due to these structures being some of the highest energy structures on the initial landscape and thus relatively few ended up in the set of candidates for active learning. Nevertheless, despite not training on many of these low density structures, considering the energy range of the landscape the uncertainties are not excessive. Overall, the potential has performed exceedingly well considering the difficulty of the landscape and has notably succeeded in learning the combined intramolecular and intermolecular correction to a high standard.

## On-the-fly Training

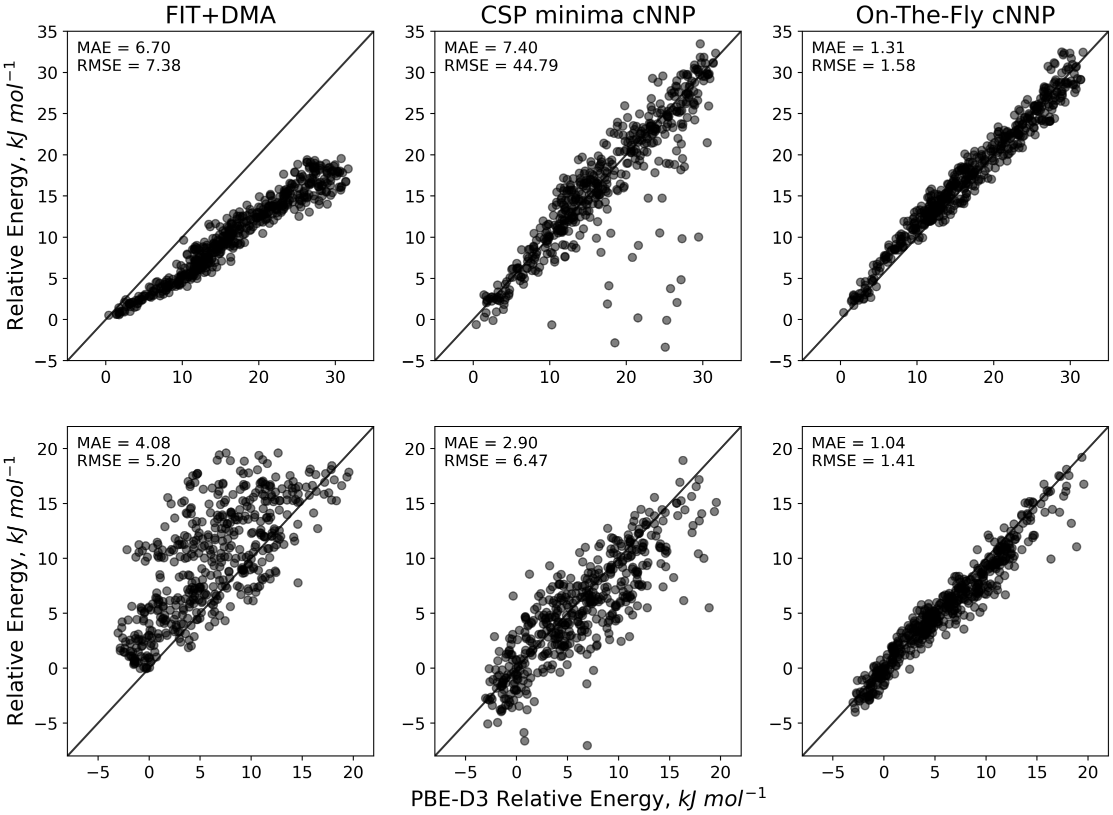

Figure 6: Correlation of FIT+DMA, CSP trained cNNP, and the CSP trained cNNP with additional Monte Carlo on-the-fly training with the PBE-D3 reference for a set of unminimized accepted structures sampled from FIT+DMA MC trajectories of the $\alpha$ (top) and $\beta$ (below) polymorphs of oxalic acid.

The potentials so far presented have been trained exclusively on energy minima of precomputed CSP landscapes and consequently have a limited description of the energy surface beyond these points. Here we look at how we can improve the description of the PES through on-the-fly training within Monte Carlo simulations. We demonstrate this using the 300 lowest energy structures from the CSP landscape predicted for oxalic acid.

Before we can begin the simulations we first need to determine which structures to sample with the MC trajectories. Ideally we want to select structures that are diverse and well-separated on the energy surface such that the simulations cover as much of the energy surface as possible with the fewest number of trajectories. Redundant structures that occupy similar regions of the energy surface will add little to improving the MLIP while increasing the computational cost. The area of the energy surface that will be covered by each trajectory is difficult to determine *a priori*, however, using farthest point sampling we can ensure that our selected structures represent a diverse set. Thus, we selected 10 structures from the set of 300 oxalic acid structures by FPS in the descriptor space starting from the lowest energy structure, which also is the match to the $\beta$ polymorph. On-the-fly training from these structures with an uncertainty threshold of 2.0 kJ mol$^{-1}$ yielded 1636 structures from the MC trajectories that were added to the training set.

To illustrate the improvement of the potential we first ran simple downhill Monte Carlo simulations on the 300 oxalic acid structures (Figure S4). These simulations, which only accept Monte Carlo moves that decrease the energy, are relatively localized, constrained effectively to the initial energy basin. Nevertheless, using the initial cNNP trained on CSP minima we find that only 9 CSP structures remain stable after 1500 MC steps. The other 291 trajectories were terminated early due to high uncertainties in energy predictions in excess of 50 kJ mol$^{-1}$. By contrast, performing the same simulations with the on-the-fly trained cNNP 299 trajectories remain stable.

To further qualify the differences in the potential, we generated a test set of 1000 unminimized structures, randomly sampled from FIT+DMA MC simulations of the $\alpha$ and $\beta$ polymorphs. The MC simulations sampled an energy up to 20 kJ mol$^{-1}$ above the initial energy and were sampled evenly such that 500 structures were from the $\alpha$ polymorph trajectory and 500 were from the $\beta$ polymorph trajectory. The correlations of energies for these structures calculated by PBE-D3 against those calculated by FIT+DMA, the cNNP trained on CSP minima, and the cNNP with on-the-fly training are shown in Figure 6. Considering first FIT+DMA, there is a notable and pronounced systematic underestimation of the energies for the $\alpha$ polymorph structures and yet simultaneously a systematic overestimation for the $\beta$ polymorph structures. These inconsistent errors reflect the difficulty in accurately capturing the oxalic acid energy surface with the simple functional form and thus emphasizes the limitations of the the FIT potential for this system.

By contrast, the cNNP trained on CSP minima does not exhibit similar systematic errors, and for most structures achieves low errors. Indeed, for the structures sampled from the $\beta$ polymorph trajectory the model achieves a significantly lower MAE than FIT+DMA. However, the limitation of this model, and the cause of the unstable downhill MC trajectories, is a small number of structures that the model returns excessively large errors for, often more than 100 kJ mol$^{-1}$. The effect of these outliers can be seen in the RMSEs, which are multiple times larger than the MAEs. Pleasingly, the uncertainties on the outlier predictions are similarly large. For example, removing structures with uncertainties above 10 kJ mol$^{-1}$ for the $\alpha$ trajectory structures, which corresponds to 72 structures (from 500 total), we find the underlying MAE and RMSE to be 1.56 and 2.03 kJ mol$^{-1}$, respectively. Therefore, while the extrapolation of the model is better than expected for the majority of structures, highlighting the broad relevance of potentials trained on CSP minima, the prevalence of outliers suggests an incomplete description of the energy surface.

Improving this description is the aim of the on-the-fly training and comparing the correlations before and after on-the-fly training there is a clear improvement. Not only are all outliers eliminated, but also the errors across the test set are significantly reduced, resulting in notably lower MAEs. Considering the $\alpha$ polymorph was not among the initial structures in the on-the-fly training, the improved accuracy for these structures is particularly impressive. For comparison, if we do include an on-the-fly simulation initiated from the $\alpha$ polymorph, the resulting model achieves an MAE of just 0.5 kJ mol$^{-1}$ on the same structures (Figure S5). The possibility to further improve the accuracy with further sampling is also evident in the subtle trend of larger errors at higher energies, which suggests the sampling at these energies could be insufficient. However, this is not unexpected considering the on-the-fly training trajectories were shorter than the trajectories the test structures were sampled from, and moreover, may have sampled different regions due to the different energy models.

Beyond accuracy, we were also interested in improving the efficiency of the on-the-fly sampling, which seemed achievable considering the generally good accuracy of the cNNP trained on CSP minima, implying that only a small number of structures with high uncertainties need to be added to the training set to yield a robust potential. To investigate this we repeated the first on-the-fly training starting from the same 10 structures but with a higher uncertainty threshold of 10 kJ mol$^{-1}$. This change resulted in only 91 structures being added to the training set, a reduction of 95% compared to the on-the-fly training with a 2 kJ mol$^{-1}$ threshold. Despite the smaller training set, the model performs well. The correlation plots of this model (Figure S6) show it still achieves a significant improvement compared to the model trained only on CSP lattice energy minima, and importantly, eliminates the outliers, which suggests a robust description of the energy surface. Of course, the average errors are not as small as with the 2 kJ mol$^{-1}$ uncertainty threshold, but considering the reduced computational cost, it could be a worthwhile compromise, allowing longer, higher energy trajectories and/or more trajectories during the on-the-fly training.

# Discussion

The diversity of structures typically found on organic CSP landscapes provides a great resource for training MLIPs that are relevant across a wide scope of the lattice energy surface. The results presented here demonstrate how active learning combined with $\Delta$-learning provides an efficient workflow to generate MLIPs from these datasets. The resulting potentials can be applied directly to correct the energies of CSP structures to higher levels of theory or can be extended by on-the-fly training within MC simulations to accurately describe the energy surface beyond the local energy minima.

The presented workflow should be generally useful for organic CSP and can help address the often prohibitive costs associated with the DFT ranking of predicted structures.[10] For instance, training to the TTBI landscape was completed at a cost of 1498 CPU hours, which is conservatively estimated to be a 155 fold reduction compared to evaluating the landscape directly at the target (PBE-D3) level of theory. In real time, this corresponds to the difference between 20 hours and 130 days using 80 Intel(R) Xeon(R) Gold 6248 CPU cores @ 2.50GHz. Similar efficiency was observed for resorcinol with the cost of the corrected landscape estimated at 1293 CPU hours. The on-the-fly sampling is likewise notably efficient. The initial sampling, which added 1636 structures to the training set, corresponds to only 3.6% of the structures evaluated during the simulations. However, as shown in the results, if willing to accept lower accuracy a similarly robust potential can be achieved with considerably less sampling and thus cost.

These results focused on achieving a first approximation of the DFT landscape, which is a common part of organic CSP workflows. For some systems higher level rankings, including free energy corrections, are important[65] In such cases, low energy structures from the MLIP corrected landscape can be selected for these calculations as is typically done. However, with further training, such as the on-the-fly training including atom forces, we envisage the MLIPs themselves could be used for these calculations. MLIPs that accurately predict vibrational spectra have been demonstrated in other studies and thus we are reasonably confident the MLIPs we have presented could be extended to high level rankings of organic crystals including free energies.

The workflow developed here is applied to a pre-computed CSP landscape. Therefore, the methodology can be applied to existing legacy or published landscapes, as well as new CSP studies. However, the requirement for a pre-computed CSP structure set means that a ‘good enough’ baseline model is required. Where the baseline is an empirically parameterized force field, molecules with less common functional groups or elements might be less well modelled by common empirical force fields; therefore, either developing tailored force field parameters or using higher level and likely more expensive methods, such as DFTB, might still be required to generate the initial landscape. A further consideration is that the potentials generated with the methods presented here are reliable at local minima on the lattice energy surface and, when on-the-fly training to Monte Carlo trajectories is included, are accurate in the local region of the lattice energy surface. Thus, as shown in the on-the-fly training results the potentials can achieve lattice energy minimizations from good starting structures. However, properties and behaviour that require a broader description of the lattice energy surface, such as transitions between polymorphs, might require the potential to extrapolate beyond its training, so risks loss of accuracy.

An alternative approach, which addresses both issues, would be to train the MLIP on-the-fly at the structure-generation stage of CSP, so that the training sees high energy configurations and can correct for deficiencies in the force field while the landscape is being generated. This type of approach has been demonstrated for inorganic CSP [25,29] where the CSP search is frequently performed at the *ab initio* level, and so leads to a stronger impetus to improve efficiency in this stage. Due to the large range of interactions explored in CSP of organic molecules, we expect that a similar approach would result in much larger training datasets relative to what is needed when aiming to model the lattice energy minima and their local regions.

Beyond the scope of the MLIPs, the variability in the active learning results is also notable. As shown in the results for oxalic acid, even when using the optimal parameters and strategy identified, we found significant variation in the training sets selected. This is especially clear when the active learning was repeated while keeping all parameters except the starting structures constant (Table S2). While ML models have inherent variability due to stochastic elements involved in training, considering the most expensive part of developing MLIPs is typically in generating the reference data, minimizing variation in the selected training set should be a priority and is worth further study.

Another area for future development is to automatically partition the lattice energy into intramolecular and intermolecular contributions, to improve the model's applicability to flexible molecules. Our results for resorcinol illustrate that a single model can accurately capture the intramolecular and intermolecular components of a landscape with limited conformations. However, other studies have found that the difference in scale between inter- and intramolecular interactions means that capturing both with a single model is often limiting, and that training separate intermolecular and intramolecular models yields improved performance.[46,66] Partitioning the energy will also make applying the workflow over multiple landscapes more practical, which could allow for training transferable rather than system-specific models. The development of universal models for organic molecules[38,67–70] and inorganic materials,[71–73] has produced impressive results with good transferability; similar models for organic crystals could have an important impact in the field of CSP.

## Conclusions

Computational efficiency is an important aspect of crystal structure prediction and its practical applications. As seen in the recent blind tests, the increasing use of high level quantum chemistry calculations for correcting initial CSP landscapes has led to dramatic increases in computational costs. Notably, these increasing costs are causing a disparity between researchers and groups that have access to large-scale computational resources and those that do not, and so limits the impact of these methods in polymorph screening, crystal engineering and materials discovery. In this context, accurate MLIPs have arrived with fortuitous timing and with the potential to reduce the cost of organic CSP without compromising on the necessary high-level accuracy.

The workflow we have presented here is a further step towards integrating MLIPs into organic CSP. By combining active learning and $\Delta$-learning, leveraging the lower level energies describing the landscapes, which are available at no added computational cost beyond the crystal structure search, we have demonstrated a highly efficient and automatable method for generating MLIPs from CSP landscapes. As shown for oxalic acid and resorcinol, active learning from a force field or DFTB baseline can achieve errors at or below 1 kJ mol$^{-1}$, using approximately 10 % of the landscape for training. We converged active learning at errors of 3-4 kJ mol$^{-1}$, as being acceptable over a much broader energy range of predicted crystal structures using only 1.2% of structures for training.

Furthermore, we have illustrated how these potentials can be readily extended to points on the lattice energy surface far from the initial CSP structures through on-the-fly training within Monte Carlo simulations. The resulting potential yielding stable crystal structure optimizations. Future studies will investigate training separate models for the intramolecular and intermolecular components towards an improved description of conformationally flexible systems, applying transfer learning and multi-fidelity approaches to reach higher levels of theory efficiently, and a more advanced training scheme to reduce variability in the active learning. Our results here further exemplify the potential of MLIPs to accelerate organic molecular CSP, and with the improvement in MLIP models and descriptors ongoing there is still much more to be realized.

## Author Contributions

P.B. wrote the active learning and on-the-fly training software, conducted the calculations and simulations, and wrote the original draft. R.H. wrote the first version of the cNNP prediction code, explored neural network parameters and initial applications to CSP landscapes. G.M.D. supervised the research. All authors contributed to the conceptualization, analysis of the results, and writing of the final manuscript.

## Conflicts of interest

There are no conflicts to declare.

# Acknowledgement

P.B. is funded by a University of Southampton Presidential Scholarship. R. H. is funded by the Engineering and Physical Sciences Research Council (EPSRC), grant EP/V026887/1. We acknowledge the Iridis5 High Performance Computing facility, and associated support services at the University of Southampton. Via our membership of the UK's HEC Materials Chemistry Consortium, which is funded by EPSRC (EP/R029431), this work used the Young HPC facility.

# Supporting Information Available

Additional methodological details and results are available in the Supporting Information document. The CSP datasets, training sets, and final cNNP parameters for oxalic acid, TTBI, and resorcinol are available at `doi.org/10.5258/SOTON/D2840`. Python code implementing the active learning strategies is available at `github.com/pwvbutler/CSP-AL`.

# References

(1) Bryant, M. J.; Black, S. N.; Blade, H.; Docherty, R.; Maloney, A. G. P.; Taylor, S. C. The CSD Drug Subset: The Changing Chemistry and Crystallography of Small Molecule Pharmaceuticals. *J. Pharm. Sci.* **2019**, *108*, 1655–1662.

(2) Walley, S. M.; Field, J. E.; Greenaway, M. W. Crystal Sensitivities of Energetic Materials. *Mater. Sci. Technol.* **2006**, *22*, 402–413.

(3) Wang, C.; Dong, H.; Jiang, L.; Hu, W. Organic Semiconductor Crystals. *Chem. Soc. Rev.* **2018**, *47*, 422–500.

(4) Bernstein, J. *Polymorphism in Molecular Crystals*; International Union of Crystallography Monographs on Crystallography; Oxford University Press: Oxford, 2007.

(5) Chemburkar, S. R. et al. Dealing with the Impact of Ritonavir Polymorphs on the Late Stages of Bulk Drug Process Development. *Org. Process Res. Dev.* **2000**, *4*, 413–417.

(6) Chung, H.; Diao, Y. Polymorphism as an Emerging Design Strategy for High Performance Organic Electronics. *J. Mater. Chem. C* **2016**, *4*, 3915–3933.

(7) Day, G. M. et al. A Third Blind Test of Crystal Structure Prediction. *Acta Cryst B* **2005**, *61*, 511–527.

(8) Day, G. M. et al. Significant Progress in Predicting the Crystal Structures of Small Organic Molecules – a Report on the Fourth Blind Test. *Acta Cryst B* **2009**, *65*, 107–125.

(9) Bardwell, D. A. et al. Towards Crystal Structure Prediction of Complex Organic Compounds – a Report on the Fifth Blind Test. *Acta Cryst B* **2011**, *67*, 535–551.

(10) Reilly, A. M. et al. Report on the Sixth Blind Test of Organic Crystal Structure Prediction Methods. *Acta Cryst B* **2016**, *72*, 439–459.

(11) Nyman, J.; Day, G. M. Static and Lattice Vibrational Energy Differences between Polymorphs. *CrystEngComm* **2015**, *17*, 5154–5165.

(12) Greenwell, C.; McKinley, J. L.; Zhang, P.; Zeng, Q.; Sun, G.; Li, B.; Wen, S.; Beran, G. J. O. Overcoming the Difficulties of Predicting Conformational Polymorph Energetics in Molecular Crystals via Correlated Wavefunction Methods. *Chem. Sci.* **2020**, *11*, 2200–2214.

(13) Wen, S.; Beran, G. J. O. Accidental Degeneracy in Crystalline Aspirin: New Insights from High-Level Ab Initio Calculations. *Cryst. Growth Des.* **2012**, *12*, 2169–2172.

(14) Price, A. J. A.; Mayo, R. A.; Otero-de-la-Roza, A.; Johnson, E. R. Accurate and Efficient Polymorph Energy Ranking with XDM-corrected Hybrid DFT. *CrystEngComm* **2023**, *25*, 953–960.

(15) Weatherby, J. A.; Rumson, A. F.; Price, A. J. A.; Otero de la Roza, A.; Johnson, E. R. A Density-Functional Benchmark of Vibrational Free-Energy Corrections for Molecular Crystal Polymorphism. *J. Chem. Phys.* **2022**, *156*, 114108.

(16) Whittleton, S. R.; Otero-de-la-Roza, A.; Johnson, E. R. Exchange-Hole Dipole Dispersion Model for Accurate Energy Ranking in Molecular Crystal Structure Prediction. *J. Chem. Theory Comput.* **2017**, *13*, 441–450.

(17) Neumann, M. A.; Leusen, F. J. J.; Kendrick, J. A Major Advance in Crystal Structure Prediction. *Angew. Chem. Int. Ed.* **2008**, *47*, 2427–2430.

(18) Hoja, J.; Tkatchenko, A. First-Principles Stability Ranking of Molecular Crystal Polymorphs with the DFT+MBD Approach. *Faraday Discuss.* **2018**, *211*, 253–274.

(19) Nyman, J.; Pundyke, O. S.; Day, G. M. Accurate Force Fields and Methods for Modelling Organic Molecular Crystals at Finite Temperatures. *Phys. Chem. Chem. Phys.* **2016**, *18*, 15828–15837.

(20) Deringer, V. L.; Caro, M. A.; Csányi, G. Machine Learning Interatomic Potentials as Emerging Tools for Materials Science. *Adv. Mater.* **2019**, *31*, 1902765.

(21) Behler, J. Four Generations of High-Dimensional Neural Network Potentials. *Chem. Rev.* **2021**, *121*, 10037–10072.

(22) Kulichenko, M.; Smith, J. S.; Nebgen, B.; Li, Y. W.; Fedik, N.; Boldyrev, A. I.; Lubbers, N.; Barros, K.; Tretiak, S. The Rise of Neural Networks for Materials and Chemical Dynamics. *J. Phys. Chem. Lett.* **2021**, *12*, 6227–6243.

(23) Unke, O. T.; Chmiela, S.; Sauceda, H. E.; Gastegger, M.; Poltavsky, I.; Schütt, K. T.; Tkatchenko, A.; Müller, K.-R. Machine Learning Force Fields. *Chem. Rev.* **2021**, *121*, 10142–10186.

(24) Clements, R. J.; Dickman, J.; Johal, J.; Martin, J.; Glover, J.; Day, G. M. Roles and opportunities for machine learning in organic molecular crystal structure prediction and its applications. *MRS Bulletin* **2022**, *47*, 1054–1062.

(25) Deringer, V. L.; Proserpio, D. M.; Csányi, G.; Pickard, C. J. Data-Driven Learning and Prediction of Inorganic Crystal Structures. *Faraday Discuss.* **2018**, *211*, 45–59.

(26) Pickard, C. J. Ephemeral Data Derived Potentials for Random Structure Search. *Phys. Rev. B* **2022**, *106*, 014102.

(27) Kapil, V.; Engel, E. A. A Complete Description of Thermodynamic Stabilities of Molecular Crystals. *Proc. Natl. Acad. Sci.* **2022**, *119*, e2111769119.

(28) Cheng, B.; Mazzola, G.; Pickard, C. J.; Ceriotti, M. Evidence for Supercritical Behaviour of High-Pressure Liquid Hydrogen. *Nature* **2020**, *585*, 217–220.

(29) Tong, Q.; Xue, L.; Lv, J.; Wang, Y.; Ma, Y. Accelerating CALYPSO Structure Prediction by Data-Driven Learning of a Potential Energy Surface. *Faraday Discuss.* **2018**, *211*, 31–43.

(30) Ko, T. W.; Finkler, J. A.; Goedecker, S.; Behler, J. A Fourth-Generation High-Dimensional Neural Network Potential with Accurate Electrostatics Including Non-Local Charge Transfer. *Nat Commun* **2021**, *12*, 398.

(31) Grisafi, A.; Ceriotti, M. Incorporating Long-Range Physics in Atomic-Scale Machine Learning. *J. Chem. Phys.* **2019**, *151*, 204105.

(32) Anstine, D. M.; Isayev, O. Machine Learning Interatomic Potentials and Long-Range Physics. *J. Phys. Chem. A* **2023**, *127*, 2417–2431.

(33) Ramakrishnan, R.; Dral, P. O.; Rupp, M.; Von Lilienfeld, O. A. Big Data Meets Quantum Chemistry Approximations: The Δ-Machine Learning Approach. *J. Chem. Theory Comput.* **2015**, *11*, 2087–2096.

(34) McDonagh, D.; Skylaris, C.-K.; Day, G. M. Machine-Learned Fragment-Based Energies for Crystal Structure Prediction. *J. Chem. Theory Comput.* **2019**, *15*, 2743–2758.

(35) Wengert, S.; Csányi, G.; Reuter, K.; T. Margraf, J. Data-Efficient Machine Learning for Molecular Crystal Structure Prediction. *Chem. Sci.* **2021**, *12*, 4536–4546.

(36) Wengert, S.; Csányi, G.; Reuter, K.; Margraf, J. T. A Hybrid Machine Learning Approach for Structure Stability Prediction in Molecular Co-crystal Screenings. *J. Chem. Theory Comput.* **2022**, *18*, 4586–4593.

(37) Egorova, O.; Hafizi, R.; Woods, D. C.; Day, G. M. Multifidelity Statistical Machine Learning for Molecular Crystal Structure Prediction. *J. Phys. Chem. A* **2020**, *124*, 8065–8078.

(38) Smith, J. S.; Nebgen, B.; Lubbers, N.; Isayev, O.; Roitberg, A. E. Less Is More: Sampling Chemical Space with Active Learning. *J. Chem. Phys.* **2018**, *148*, 241733.

(39) Artrith, N.; Behler, J. High-Dimensional Neural Network Potentials for Metal Surfaces: A Prototype Study for Copper. *Phys. Rev. B* **2012**, *85*, 045439.

(40) Sivaraman, G.; Krishnamoorthy, A. N.; Baur, M.; Holm, C.; Stan, M.; Csányi, G.; Benmore, C.; Vázquez-Mayagoitia, Á. Machine-Learned Interatomic Potentials by Active Learning: Amorphous and Liquid Hafnium Dioxide. *npj Comput Mater* **2020**, *6*, 1–8.

(41) Liu, P.; Wang, J.; Avargues, N.; Verdi, C.; Singraber, A.; Karsai, F.; Chen, X.-Q.; Kresse, G. Combining Machine Learning and Many-Body Calculations: Coverage-Dependent Adsorption of CO on Rh(111). *Phys. Rev. Lett.* **2023**, *130*, 078001.

(42) Lookman, T.; Balachandran, P. V.; Xue, D.; Yuan, R. Active Learning in Materials Science with Emphasis on Adaptive Sampling Using Uncertainties for Targeted Design. *npj Comput Mater* **2019**, *5*, 1–17.

(43) Podryabinkin, E. V.; Shapeev, A. V. Active Learning of Linearly Parametrized Interatomic Potentials. *Comput. Mater. Sci.* **2017**, *140*, 171–180.

(44) Vandermause, J.; Torrisi, S. B.; Batzner, S.; Xie, Y.; Sun, L.; Kolpak, A. M.; Kozinsky, B. On-the-Fly Active Learning of Interpretable Bayesian Force Fields for Atomistic Rare Events. *npj Comput Mater* **2020**, *6*, 1–11.

(45) Zhang, Y.; Wang, H.; Chen, W.; Zeng, J.; Zhang, L.; Wang, H.; E, W. DP-GEN: A Concurrent Learning Platform for the Generation of Reliable Deep Learning Based Potential Energy Models. *Comput. Phys. Commun.* **2020**, *253*, 107206.

(46) A. Young, T.; Johnston-Wood, T.; L. Deringer, V.; Duarte, F. A Transferable Active-Learning Strategy for Reactive Molecular Force Fields. *Chem. Sci.* **2021**, *12*, 10944–10955.

(47) Schran, C.; Brezina, K.; Marsalek, O. Committee Neural Network Potentials Control Generalization Errors and Enable Active Learning. *J. Chem. Phys.* **2020**, *153*, 104105.

(48) Hafizi, R.; Elsner, J.; Blumberger, J. Ultrafast Electronic Coupling Estimators: Neural Networks versus Physics-Based Approaches. *J. Chem. Theory Comput.* **2023**, *19*, 4232–4242.

(49) Butler, P. W. V.; Day, G. M. Reducing Overprediction of Molecular Crystal Structures via Threshold Clustering. *Proc. Natl. Acad. Sci.* **2023**, *120*, e2300516120.

(50) Zhu, Q.; Johal, J.; Widdowson, D. E.; Pang, Z.; Li, B.; Kane, C. M.; Kurlin, V.; Day, G. M.; Little, M. A.; Cooper, A. I. Analogy Powered by Prediction and Structural Invariants: Computationally Led Discovery of a Mesoporous Hydrogen-Bonded Organic Cage Crystal. *J. Am. Chem. Soc.* **2022**, *144*, 9893–9901.

(51) Case, D. H.; Campbell, J. E.; Bygrave, P. J.; Day, G. M. Convergence Properties of

Crystal Structure Prediction by Quasi-Random Sampling. *J. Chem. Theory Comput.* **2016**, *12*, 910–924.

(52) Williams, D. E.; Cox, S. R. Nonbonded Potentials for Azahydrocarbons: The Importance of the Coulombic Interaction. *Acta Cryst B* **1984**, *40*, 404–417.

(53) Coombes, D. S.; Price, S. L.; Willock, D. J.; Leslie, M. Role of Electrostatic Interactions in Determining the Crystal Structures of Polar Organic Molecules. A Distributed Multipole Study. *The Journal of Physical Chemistry* **1996**, *100*, 7352–7360.

(54) Beyer, T.; Price, S. L. Dimer or Catemer? Low-Energy Crystal Packings for Small Carboxylic Acids. *The Journal of Physical Chemistry B* **2000**, *104*, 2647–2655.

(55) Stone, A. J. Distributed Multipole Analysis: Stability for Large Basis Sets. *Journal of Chemical Theory and Computation* **2005**, *1*, 1128–1132, PMID: 26631656.

(56) Behler, J.; Parrinello, M. Generalized Neural-Network Representation of High-Dimensional Potential-Energy Surfaces. *Phys. Rev. Lett.* **2007**, *98*, 146401.

(57) Singraber, A.; Morawietz, T.; Behler, J.; Dellago, C. Parallel Multistream Training of High-Dimensional Neural Network Potentials. *J. Chem. Theory Comput.* **2019**, *15*, 3075–3092.

(58) Singraber, A.; Behler, J.; Dellago, C. Library-Based LAMMPS Implementation of High-Dimensional Neural Network Potentials. *J. Chem. Theory Comput.* **2019**, *15*, 1827–1840.

(59) Imbalzano, G.; Anelli, A.; Giofré, D.; Klees, S.; Behler, J.; Ceriotti, M. Automatic Selection of Atomic Fingerprints and Reference Configurations for Machine-Learning Potentials. *J. Chem. Phys.* **2018**, *148*, 241730.

(60) Yang, S.; Day, G. M. Global Analysis of the Energy Landscapes of Molecular Crystal Structures by Applying the Threshold Algorithm. *Commun Chem* **2022**, *5*, 1–13.

(61) Nobeli, I.; Price, S. L. A Non-Empirical Intermolecular Potential for Oxalic Acid Crystal Structures. *J. Phys. Chem. A* **1999**, *103*, 6448–6457.

(62) Mastalerz, M.; Oppel, I. M. Rational Construction of an Extrinsic Porous Molecular Crystal with an Extraordinary High Specific Surface Area. *Angewandte Chemie International Edition* **2012**, *51*, 5252–5255.

(63) Pulido, A. et al. Functional Materials Discovery Using Energy–Structure–Function Maps. *Nature* **2017**, *543*, 657–664.

(64) McMahon, D. P.; Stephenson, A.; Chong, S. Y.; Little, M. A.; Jones, J. T. A.; Cooper, A. I.; Day, G. M. Computational Modelling of Solvent Effects in a Prolific Solvatomorphic Porous Organic Cage. *Faraday Discuss.* **2018**, *211*, 383–399.

(65) Taylor, C. R.; Mulvee, M. T.; Perenyi, D. S.; Probert, M. R.; Day, G. M.; Steed, J. W. Minimizing Polymorphic Risk through Cooperative Computational and Experimental Exploration. *Journal of the American Chemical Society* **2020**, *142*, 16668–16680, PMID: 32897065.

(66) Magdău, I.-B.; Arismendi-Arrieta, D. J.; Smith, H. E.; Grey, C. P.; Hermansson, K.; Csányi, G. Machine Learning Force Fields for Molecular Liquids: Ethylene Carbonate/Ethyl Methyl Carbonate Binary Solvent. *npj Comput Mater* **2023**, *9*, 1–15.

(67) S. Smith, J.; Isayev, O.; E. Roitberg, A. ANI-1: An Extensible Neural Network Potential with DFT Accuracy at Force Field Computational Cost. *Chem. Sci.* **2017**, *8*, 3192–3203.

(68) Smith, J. S.; Nebgen, B. T.; Zubatyuk, R.; Lubbers, N.; Devereux, C.; Barros, K.; Tretiak, S.; Isayev, O.; Roitberg, A. E. Approaching Coupled Cluster Accuracy with a General-Purpose Neural Network Potential through Transfer Learning. *Nat Commun* **2019**, *10*, 2903.

(69) Zubatyuk, R.; Smith, J. S.; Leszczynski, J.; Isayev, O. Accurate and Transferable Multitask Prediction of Chemical Properties with an Atoms-in-Molecules Neural Network. *Sci. Adv.* **2019**, *5*, eaav6490.

(70) Gasteiger, J.; Becker, F.; Günnemann, S. GemNet: Universal Directional Graph Neural Networks for Molecules. *Adv. Neural Inf. Process. Syst.* **2021**, *34*, 6790–6802.

(71) Deng, B.; Zhong, P.; Jun, K.; Riebesell, J.; Han, K.; Bartel, C. J.; Ceder, G. CHGNet as a Pretrained Universal Neural Network Potential for Charge-Informed Atomistic Modelling. *Nat Mach Intell* **2023**, *5*, 1031–1041.

(72) Choudhary, K.; DeCost, B.; Major, L.; Butler, K.; Thiyagalingam, J.; Tavazza, F. Unified Graph Neural Network Force-Field for the Periodic Table: Solid State Applications. *Digital Discovery* **2023**, *2*, 346–355.

(73) Chen, C.; Ong, S. P. A Universal Graph Deep Learning Interatomic Potential for the Periodic Table. *Nat Comput Sci* **2022**, *2*, 718–728.

TOC Graphic

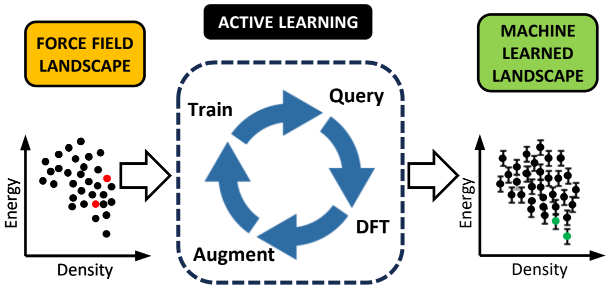
FORCE FIELD LANDSCAPE
Energy
Density
ACTIVE LEARNING
Train
Query
DFT
Augment
MACHINE LEARNED LANDSCAPE
Energy
Density